Spatially Constrained Random Walk Approach for Accurate Estimation of Airway Wall Surfaces

Ziyue Xu*, Ulas Bagci, Brent Foster, Awais Mansoor, and Daniel J. Mollura

Center for Infectious Disease Imaging (CIDI)
Department of Radiology and Imaging Sciences
National Institutes of Health (NIH), Bethesda, MD 20892, USA

Abstract. Assessing airway wall surfaces and the lumen from high resolution computed tomography (CT) scans are of great importance for diagnosing pulmonary diseases. However, accurately determining inner and outer airway wall surfaces of a complete 3-D tree structure can be quite challenging because of its complex nature. In this paper, we introduce a computational framework to accurately quantify airways through (i) a precise segmentation of the lumen, and (ii) a spatially constrained Markov random walk method to estimate the airway walls. Our results demonstrate that the proposed airway analysis platform identified the inner and outer airway surfaces better than methods commonly used in clinics, such as full width at half maximum and phase congruency.

Keywords: lumen segmentation, airway wall estimation, fuzzy connectivity, random walk, full width at half maximum, phase congruency.

1 Introduction

Airways are pathologically involved in various lung diseases, and CT imaging enables a quantitative investigation of airways; however, in clinical practice, the airway wall thickness is roughly measured at limited locations by radiologists, and an accurate measurement of airway dimensions has remained a salient task due to the complexity of airway structures. A precise method for airway segmentation and an accurate estimation of airway wall thickness may facilitate better quantification of airway pathologies, further enhancing the understanding of mechanism of the disease progression.

Prior Work: Although recently there has been many attempts to accurately measure airway structures and walls, we explain *two most widely applied techniques* herein, full width at half maximum (FWHM) [1] and phase congruency [2], respectively. FWHM defines the wall boundary at the location where the intensity is half the peak value within the wall. However, this measurement can be biased due to partial volume effect and CT reconstruction. Furthermore, FWHM may leak to surrounding structures with the presence of adjacent vessels. Phase congruency [2], on the other hand, was conceived as a model-free alternative with edge locations identified by maximal local

* Corresponding author: ziyue.xu@nih.gov. This research is supported by CIDI, the intramural research program of the National Institute of Allergy and Infectious Diseases (NIAID) and the National Institute of Biomedical Imaging and Bioengineering (NIBIB).

K. Mori et al. (Eds.): MICCAI 2013, Part II, LNCS 8150, pp. 559–566, 2013.

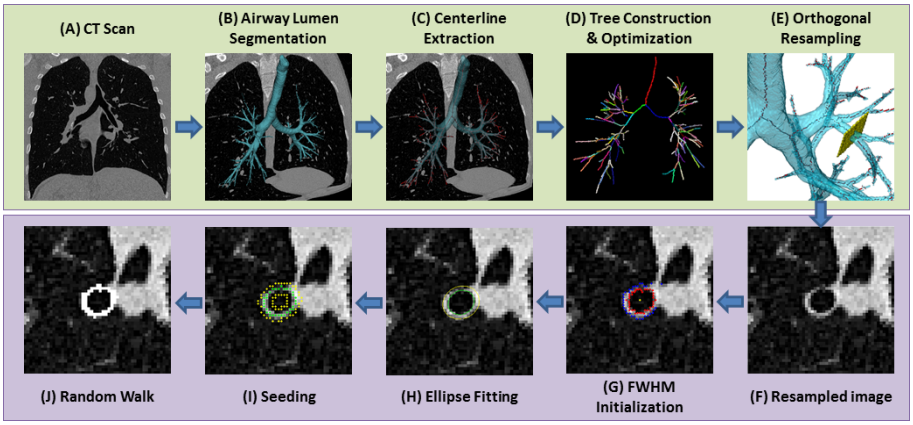

Fig. 1. Flowchart of the airway lumen segmentation and wall estimation algorithm

phase coherency. This method is shown to be robust, but it is computationally intensive and accuracy for small airways is limited by resolution.

In this paper, we present an automatic method for airway analysis to precisely estimate inner and outer airway wall surfaces. Fig. 1 illustrates the flowchart of the proposed scheme. First, we segmented the lumen area (Fig. 1B) of the airway from CT scans (Fig. 1A) using a hybrid multi-scale approach based on fuzzy connectivity (FC) [3]. Then, we extracted the tree skeleton (Fig. 1C) from the binary image using a thinning algorithm and optimized the resulting skeleton using a graph-based dynamic programming method (Fig. 1D). Next, 2-D orthogonal samples were generated along every branch of the airway skeleton (Fig. 1E). On the 2-D orthogonal images (Fig. 1F), FWHM was performed to roughly identify the range of the lumen, the airway wall, and the parenchyma (Fig. 1G); an ellipse fitting process was added to improve estimation (Fig. 1H). Seeds (Fig. 1I) for the lumen, airway wall, and parenchyma were determined automatically to initiate random walk segmentation (Fig. 1J). In the next section, we present our proposed framework in detail.

2 Methods

Airway Lumen Segmentation Using Novel Affinity Function: We used a novel *fuzzy affinity* relationship to restrict the FC segmentation [3] to airway regions by using multiple strategies in order to achieve a *high sensitivity* with lower leakage. First, a seed at the trachea was identified automatically by 2-D Hough transform, and then a gray-scale morphological reconstruction [4] and vesselness [5] were computed and passed together with the seed to the FC computation. Our motivation for this combination within the FC framework was to help identify the airway structures and provide continuity of the airway boundary. For the algorithm discussed here, three features are available to describe a given voxel x: intensity $I(x)$, grayscale morphological reconstructed result $D(x)$ and vesselness measurement $V(x)$ such that $F(x) = \{I(x), D(x), V(x)\}$. The local scale

information, $ls(x)$, provided by the multi-scale vesselness computation, gives *additional control* over the design of the affinity function since pure intensity information is not reliable for small airway identification; the other two features yield support. The novel affinity function contains the affinities $\mu^{I}_{\psi/\phi}$, $\mu^{D}_{\psi/\phi}$, and $\mu^{V}_{\psi/\phi}$ corresponding to $I(x)$, $D(x)$ and $V(x)$, and it was constructed as:

$$\mu^{FC}_{\psi/\phi} = \begin{cases} \mu^{I}_{\psi/\phi}, & \text{if } ls > ls^{T}; \\ k\mu^{I}_{\psi/\phi} + (1-k)\sqrt{\mu^{D}_{\psi/\phi}\mu^{V}_{\psi/\phi}}, & \text{otherwise,} \end{cases} \tag{1}$$

where ls^{T} is the threshold for determining large airways; where intensity is reliable, and k is a weighing parameter, $k \in [0, 1]$, used to define small airways. k may be formulated as $k = ls/ls_{\max}$ to indicate either large or small airways ($ls_{\max}$ is a free parameter). Intuitively, vesselness and morphological constraints can be jointly modeled for identification of small airways; therefore, we incorporated their affinities in multiplicative form in the new affinity function. Free parameters, T and k, were learned in a training set of images, which are different than the test images, prior to the segmentation procedure. Due to limited space, we encourage readers to refer to [3] for the general form for affinities and their descriptions that we followed and modeled.

Centerline Extraction and Orthogonal Resampling: The tree skeleton was extracted from the segmented lumen using a binary thinning algorithm. Since the tree produced by the thinning algorithm often contained small branches corresponding to local morphological variation, rather than real branching, a graph-based dynamic programming method was employed to optimize the resulting tree by removing the small branches, similar to the optimization used in [6]. Smoothing was performed on each segment to avoid sharp changes in local tangent orientation along the skeleton, and the original CT image was then resampled into 2-D images within a neighborhood on the orthogonal planes. 2-D system can be adapted to clinical routine easily. Note that after 2-D segmentation, we followed the conventional 2-D to 3-D conversion procedure in the previous 2-D based methods in the literature [2] to generate 3-D structures based on 2-D orthogonal samples at final step. Bifurcation points were also handled similar to the previous 2-D based methods.

Spatially Constrained Markov Random Walk for Airway Wall Estimation: Lumen segmentation identifies airways as much as possible, but it can compromise the wall position locally. Therefore, we further applied local wall estimation to refine the location of both inner and outer walls. The random walk (RW) algorithm has been a widely used graph-based image segmentation method [7]. In RW, the image is considered a graph (G), which is represented as a pair, $G = (V, E)$, with nodes $v \in V$ and edges $e \in E \subseteq V$ x V. Conventionally, a node v_i is said to be a neighbor of another node, v_j, if they are connected by an edge e_{ij} in G, and each edge is weighted by w_{ij}. Although RW *usually* avoids the noisy or fragmented segmentation, it has been recently shown in [7] that this property does not always hold. Similarly, in airway wall surface segmentation, fragmented segmentation can likely occur due to similar intensity profiles of the airway walls and the nearby structures; therefore, one needs to be sure to place an *adequate number* of seeds in *suitable places*. To avoid a "connectedness" problem in this

study and provide an accurate estimation of inner and outer wall surfaces, we created a computationally efficient random walk estimation method by automatically identifying foreground and background seeds that spatially constrain random walkers. Our algorithm uses conventional FWHM and least square ellipse fitting methods to *roughly* identify the foreground and background seed locations. Furthermore, background seeds are connected so that they form 2-D convex bodies in the vicinity of outer and inner walls; therefore, hits-and-runs of random walks are restricted to no "connectedness" issue when it converges to outer and inner surface locations. Other than the automatically localized background and foreground seeds and their spatial alignment within the two ellipses (Fig. 2B), the rest of the combinatorial Dirichlet problem was solved, as indicated in [7]. Although the aim is to classify a large number of unlabeled voxels with a limited number of labeled voxels in conventional RW segmentation; herein, we classify a relatively small number of unlabeled voxels, with a large number of labeled voxels distributed over two convex surfaces (Fig. 2A, B, and C). The proposed framework allows random walkers to exploit the airway wall structures within two convex surfaces (i.e., S_1 and S_2 in short) in a robust and computationally efficient way (See Fig. 2).

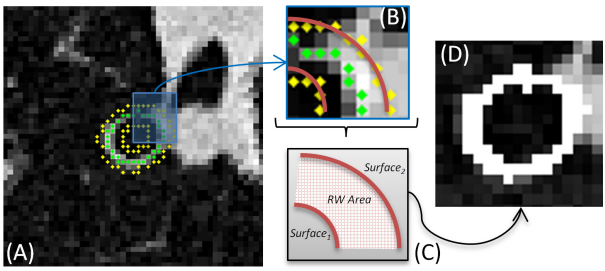

Fig. 2. (A) Airway wall with background (yellow) and foreground (green) seeds, and its zoomed version (B) are seen. (C) Background seeds form inner and outer surfaces as constraints for RW. (D) Resulting RW segmentation.

Since we incorporated strict spatial constraints to RW by using FWHM and least square ellipse fitting to identify foreground and background seed locations automatically, it is our interest to demonstrates the advantages of using strict spatial constraints by introducing soft constraints concept in RW. Assuming a set of nodes $v \in \mathcal{F} \subset V$ labeled as foreground, a set of nodes $v \in S_1 \subset V$ labeled as background (on inner surface), and a set of nodes $v \in S_2 \subset V$ labeled as background (on outer surface) such that $\mathcal{F} \cap S_1 = \emptyset$, $\mathcal{F} \cap S_2 = \emptyset$. For any $v \in \mathcal{F}$, $P(v) = 1$, and for any $v \in S_1$ or $v \in S_2$, $P(v) = 0$. For any of the remaining nodes $v \in V \setminus (\mathcal{F} \cup S_1 \cup S_2)$, $P(v) = \sum_{e_{ij} \in E} w_{ij} P(v_j)$. Conventionally, nodes with probability values greater than 0.5 (hard constraint) are classified as the foreground. Now, assuming a node is imposed a soft constraint instead of a hard constraint, the difference between a probability of a node and 0.5 is within a small prescribed range $[-\epsilon, \epsilon]$. Then, $|P(v) - 0.5| \leq \epsilon$ for $v \in V \setminus (\mathcal{F} \cup S_1 \cup S_2)$. By imposing soft constraints, the RW can be considered as a minimization problem,

$$\min \sum_{e_{ij} \in E} w_{ij} |P(v_i) - P(v_j)|^2 + \sum_{v_i \in V \setminus (\mathcal{F} \cup S_1 \cup S_2)} \lambda_i |P(v_i) - 0.5|^2 \qquad (2)$$

such that $|P(v) - 0.5| \leq \epsilon$ for $v \in V \setminus (\mathcal{F} \cup S_1 \cup S_2)$, and $P(v) = 0$ for $v \in S_1$ or $v \in S_2$, and λ is controlling the weight of the nodes with soft constraints. A detailed solution of this quadratic problem is outside the scope of this paper, however, by differing the ϵ value in the same segmentation settings, one can analyze the effect of the spatial constraints on the RW. The parameters are described in Section 3, along with detailed explanations of the quantitative results.

3 Experiments and Results

Data and Evaluation of Lumen Segmentation: We used the data set from the EXACT'09 airway segmentation challenge [8], consisting of 20 subjects covering a large variety of diseases. Binary segmentations were submitted to organizers, and the resulting evaluation statistics was sent back to us. For the evaluation of lumen segmentation results, we used the EXACT'09 criteria, as explained in the challenge [8]. We obtained an average branch count of 128.67 ± 58.68, with a detection rate of $51.74 \pm 10.55\%$. False positive rate was found to be $0.85 \pm 1.54\%$. Based on the highest tree length detected under the restriction that false positive rate is less than 1%, our approach replaces the second best method among all other methods involved in the EXACT'09 competition. Indeed, our method exhibited a much higher efficiency (20 minutes) than the top ranked method (90 minutes) in terms of the computational burden.

Evaluation of Airway Wall Surface Estimation: We selected 300 images that contained airways of different sizes under different imaging and anatomical conditions from the orthogonal resampled 2-D images generated from the EXACT'09 data set. Segmentations of these images were produced by two independent experts (i.e., Observer 1 and 2) as surrogates of the ground truth. Dice similarity coefficients (DSCs) and Hausdorff distances (HDs) were calculated for accuracy evaluation as well as inter-observer variance. With respect to the two surrogate truths, DSCs were found to be 73.9% and 81.4% with HDs of 1.82 mm and 1.61 mm; inter-observer agreement was found to be 77.6% and 1.74 mm. As initialization, FWHM method yields an accuracy of 57.5% and 64.5% with HDs of 3.56 mm and 3.35 mm, with respect to the surrogate truths; and ellipse fitting promotes the result to 58.6% and 65.2% with HDs of 2.44 mm and 2.25 mm. Qualitative comparison with the FWHM and phase congruency methods is shown in Fig. 4A-D. As illustrated, our proposed method (Fig. 4D) successfully avoided leakage and false positives in FWHM and phase congruency (Fig. 4B and C), respectively.

Airways are inherently a circular structure, thus local segmentation appearance is expected to favor circular shape rather than spiculated, which provides information for segmentation quality or local pathology. Therefore, we also used isoperimetric inequality metric (IPI) as a complementary measure to DSC. IPI is defined as $|4\pi A_i - (\mathcal{L}_i)^2|$, $i = 1, 2$, for inner $(i = 1)$ and outer $(i = 2)$ surface estimation, respectively, where A_i denotes the area enclosed by the surface S_i, and $\mathcal{L}_i$ represents the boundary length of the

corresponding A_i. In Fig. 3, estimated inner and outer boundaries of the airway walls were compared to surrogate truths, provided by Observer 1 and Observer 2, through Bland-Altman plots in column 1 and 2, respectively. As can be seen, high correlations were obtained when we compared our proposed method to observer evaluations. The third row in the figure indicates the inter-observer agreement for inner and outer wall boundary localization based on IPI measurement (the rate was found to be 75.27%). In the last row, estimated wall areas for all selected slices were compared to surrogate truths, and resulting values were plotted in ascending order. Note that the airway wall areas estimated by the proposed method are highly correlated with observers' evaluations (correlations values of $R^2 = 0.924$ and $R^2 = 0.931$ were obtained respectively).

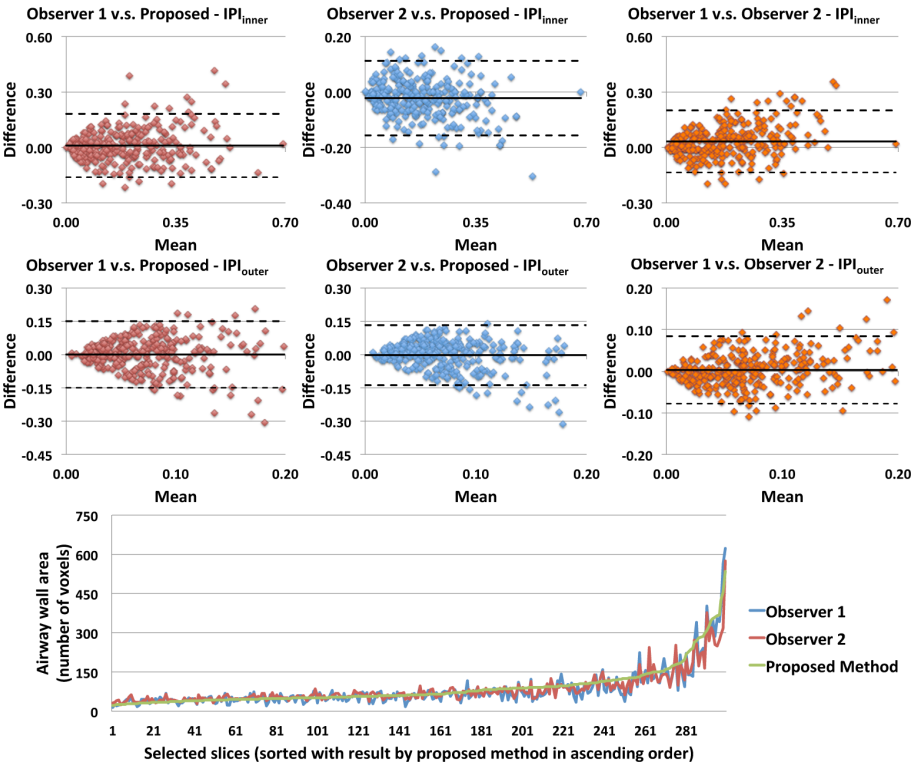

Fig. 3. First two rows show Bland-Altman plots for IPI_{inner} (first) and IPI_{outer} (second) measurements across observers and the proposed method. The last row demonstrates the agreement curve of airway wall area measurements by the proposed method and the two expert observers

Sensitivity Analysis with Respect to Seeds and Soft Constraint: As FWHM and ellipse fitting methods were used to *roughly* identify the foreground and background seed locations, it was in our interest to find the sensitivity of the constrained RW method, with respect to changes in the FWHM method. We selected 30 samples from the 300 images to assess the robustness of background seeds belonging to S_1 and S_2. Once the

FWHM method roughly estimated the wall boundary and thickness, foreground seeds were distributed halfway between S_1 and S_2. For sensitivity analysis, we redistributed the background seeds based on the convex surfaces at different distances (i.e., S_1' and S_2'). Scale parameters n_1 and n_2 were used to define the new location of the convex surfaces, $d_1 = n_1 \cdot d_{\text{wall}}$ and $d_2 = n_2 \cdot d_{\text{wall}}$. The robustness of the proposed method, with regard to seed selection, was evaluated using different values for n_1 and n_2.

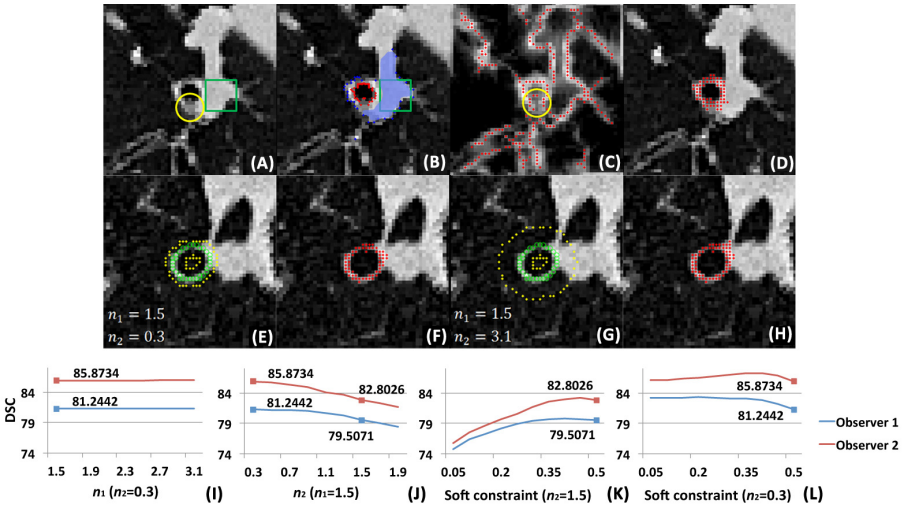

Fig. 4. (A) Original image; (B) FWHM method, dots shows boundary (block shows part of the blue leaked region); (C) phase congruency method, dots shows identified edge points, circle shows false edge caused by wall intensity inhomogeneity; (D) constrained RW successfully avoided above problems. (E, G) Seed locations with two different sets of outer seeds for a specific slice; (F, H) corresponding segmentation result for the two seed locations; (I) DSCs with changing inner seeds; (J) DSCs with changing outer seeds. (K) When outer surface is relaxed ($n_1 = 1.5, n_2 = 1.5$), segmentation accuracy started to change considerably for $\epsilon \geq 0.15$; (L) when spatially constrained RW was used ($n_1 = 1.5, n_2 = 0.3$), soft constraints did not change the segmentation results considerably even for large ϵ change

Since the lumen has a high contrast difference against neighboring structures, the background seeds on S_1 were placed when $n_1 \geq 1.5$. On the other hand, anatomical structures outside the airway wall are much more complex, so we placed the background seeds on S_2' when $n_2 \geq 0.3$. DSCs were computed for every case, and the result is shown in Fig. 4E-J. Blue and red in the figure show the segmentation results with respect to the surrogate truths provided by Observer 1 and 2, respectively. As expected, changing the location of inner background seeds did not influence the segmentation result (Fig. 4I). Placing the outer background seeds away from the airway wall can decrease the accuracy of segmentation (Fig. 4J) since adjacent structures can be falsely included, whereas such change was not as dramatic as leakage into neighboring

structures. The segmentation result was still constrained within a reasonable margin, when n_2 was large, as shown in (Fig. 4E-H).

For RW soft constraint under different spatial initialization, Fig. 4K shows RW segmentation accuracies through DSCs, where relaxing strict spatial constraints ($n_2 = 1.5$) is affecting segmentation results considerably (even for small ϵ). On the other hand, Fig. 4L shows that our spatially constrained RW segmentation method ($n_2 = 0.3$), with additional soft constraints, are incorporated as a threshold value in the RW. Note that soft constraints did not change the segmentation results considerably even for large ϵ. This indicate that the spatially constrained RW is a stable and robust method for finding boundaries of inner and outer surfaces, and sensitivity of the boundary localization is high even when spatial constraints are not strict.

4 Discussion and Conclusion

Comparison of FWHM and phase congruency methods in the literature reveals that phase congruency may identify inner and outer surfaces of airway walls better, hence, seeding locations may be more precise if the phase congruency method is used instead of FWHM. An accurate comparison of these methods within the spatially constrained RW method are left as an extension of this study.

In conclusion, we designed and developed a novel algorithm to accurately quantify airways. Specifically, this approach was based on fuzzy connectivity for precise segmentation of the airway lumen, and a spatially constrained Markov random walk method was designed to estimate the airway wall surfaces. Experiments demonstrated that our airway analysis platform gave promising results for identification of the airway surfaces.

References

1. Amirav, I., Kramer, S.S., Grunstein, M.M., Hoffman, E.A.: Assessment of methacholine-induced airway constriction by ultrafast high-resolution computed tomography. J. Appl. Physiol. 75(5), 2239–2250 (1993)
2. Estépar, R.S.J., Washko, G.G., Silverman, E.K., Reilly, J.J., Kikinis, R., Westin, C.-F.: Accurate airway wall estimation using phase congruency. In: Larsen, R., Nielsen, M., Sporring, J. (eds.) MICCAI 2006. LNCS, vol. 4191, pp. 125–134. Springer, Heidelberg (2006)
3. Udupa, J.K., Samarasekera, S.: Fuzzy connectedness and object definition: Theory, algorithms, and applications in image segmentation. CVGIP: Graph. Model & Imag. Proc. 58(3), 246–261 (1996)
4. Aykac, D., Hoffman, E.A., McLennan, G., Reinhardt, J.M.: Segmentation and analysis of the human airway tree from three-dimensional X-ray CT images. IEEE Trans. Med. Imag. 22(8), 940–950 (2003)
5. Frangi, A.F., Niessen, W.J., Vincken, K.L., Viergever, M.A.: Multiscale vessel enhancement filtering. In: Wells, W.M., Colchester, A.C.F., Delp, S.L. (eds.) MICCAI 1998. LNCS, vol. 1496, pp. 130–137. Springer, Heidelberg (1998)
6. Xu, Z., Zhao, F., Bhagalia, R., Das, B.: Generic rebooting scheme and model-based probabilistic pruning algorithm for tree-like structure tracking. In: ISBI 2012, pp. 796–799 (2012)
7. Cheng, M., Zhang, G.: Connectedness of random walk segmentation. IEEE Trans. Patt. Ana. and Mach. Intelli. 33(1), 200–202 (2011)
8. Lo, P., van Ginneken, B., Reinhardt, J., de Bruijne, M.: Extraction of airways from CT (EXACT 2009). In: Second International Workshop on Pulmonary Image Analysis, pp. 175–189 (2009)